SANDIA REPORT

SAND2014-18791
Unlimited Release
Printed September 2014

Single Atom Deposition

Grant W. Biedermann, and Weng W. Chow

Prepared by
Sandia National Laboratories
Albuquerque, New Mexico 87185 and Livermore, California 94550

Sandia National Laboratories is a multi-program laboratory managed and operated by Sandia Corporation, a wholly owned subsidiary of Lockheed Martin Corporation, for the U.S. Department of Energy's National Nuclear Security Administration under contract DE-AC04-94AL85000.

Issued by Sandia National Laboratories, operated for the United States Department of Energy by Sandia Corporation.

Available to DOE and DOE contractors from
U.S. Department of Energy
Office of Scientific and Technical Information
P.O. Box 62
Oak Ridge, TN 37831

Telephone: (865) 576-8401
Facsimile: (865) 576-5728
E-Mail: reports@adonis.osti.gov
Online ordering: http://www.osti.gov/bridge

Available to the public from
U.S. Department of Commerce
National Technical Information Service
5285 Port Royal Rd.
Springfield, VA 22161

Telephone: (800) 553-6847
Facsimile: (703) 605-6900
E-Mail: orders@ntis.fedworld.gov
Online order: http://www.ntis.gov/help/ordermethods.asp?loc=7-4-0#online

SAND2014-18791
Unlimited Release
Printed September 2014

Single Atom Deposition

Grant W. Biedermann, and Weng W. Chow
Physics-Based Microsystems, and Quantum Phenomena
Sandia National Laboratories
P.O. Box 5800
Albuquerque, New Mexico 87185-MS1082

Abstract

We have theoretically and experimentally investigated the possibility of single atom deposition using laser cooled sources. In our theoretical work, we investigated an atom source composed of out-coupling from a Bose-Einstein condensate in a trap. A model was developed for Bose-Einstein-condensate-based devices. To illustrate its application, a 2-well system is studied. The results show interesting and possibly useful differences between operation with coherent (phased-locked) and incoherent (unlocked) population transfer between levels in the two wells. The two modes of operation are governed by an interplay among scattering, energy renormalizations and coupling between wells. In parallel, we have experimentally investigated the possibility of controlled deposition of single cesium atoms onto surfaces using optical tweezers. We have measured the rate limit for translation of single atoms in optical tweezers to be 45 mm/s for stepped translation, and have constructed an apparatus for deposition of single atoms on a sapphire substrate for future work.

ACKNOWLEDGMENTS

We acknowledge experiment support from Akash Rakholia and Yuan-Yu Jau. This work was funded by Laboratory Directed Research and Development.

CONTENTS

FIGURES

NOMENCLATURE

AOM	Acousto-Optical Modulator
MOT	Magneto-Optical Trap
BEC	Bose-Einstein condensation

1. INTRODUCTION

A new generation of optoelectronic devices are being intensely investigated that will set new noise and size limits and perform functions beyond the capability of classical (Maxwell equation) light. An important example is a single-quantum-dot source for QKD, quantum computing, and single-photon generation. For these applications, precise placement of the quantum dot at the center of a microcavity is essential. Presently, one only accomplishes this with yield unacceptable for wafer-level production. Limitations come from density, flux or spatial uncertainties from a classical source. We are pursuing a leap in improvement by developing cold-atom sources for device fabrication. Our efforts have focused in parallel on the development of an experimental demonstration and theoretical modeling of future sources.

The experimental effort is developing controlled deposition and detection of single cesium atoms on a substrate. This is the simplest demonstration of the control that is required to place individual atoms at precise locations, and will open the door for other elements that can be cooled and trapped. The theoretical investigation has modeled a forward-looking improved cold atom source for deterministically placing single atoms.

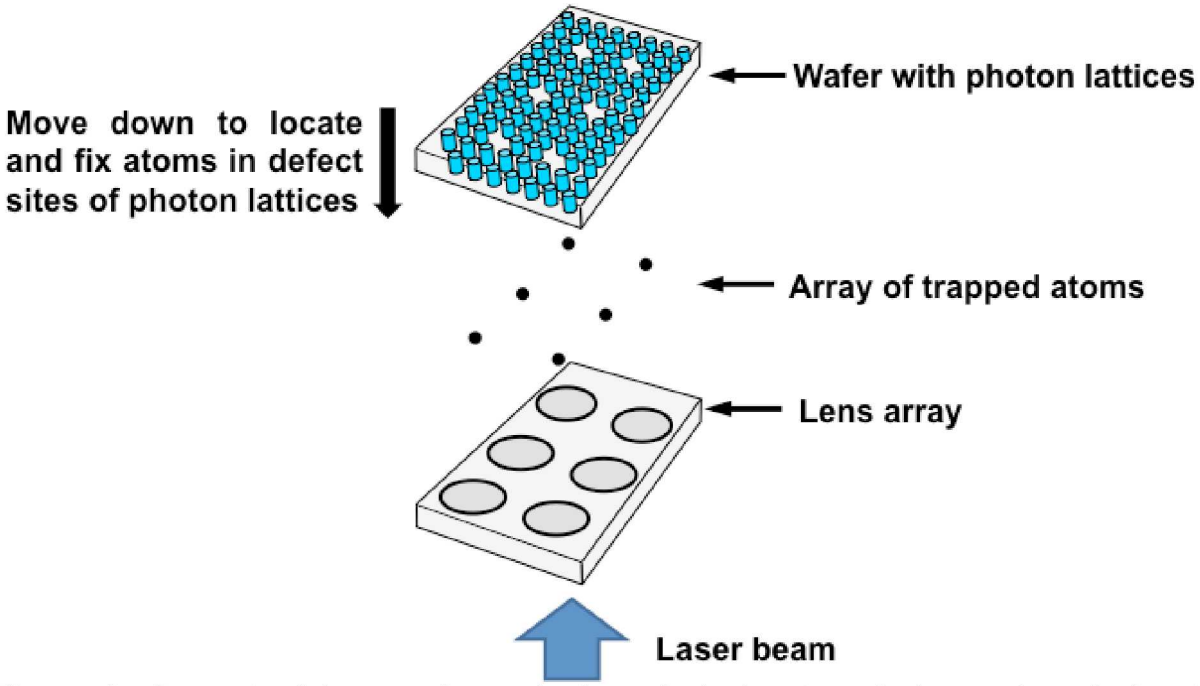

Figure 1: Concept of large-scale production of single atom devices using single atom deposition. An array of trapped atoms is generated using laser cooled atoms loaded into an array of optical tweezers. An aligned substrate is then translated to receive the single atoms at appropriate locations.

A long-term vision for large-scale implementation includes an array of traps using micro lenses that stamps single atoms onto a substrate (see Fig. 1). These traps may consist of either single atom tweezers or Bose-Einstein condensates (BEC) with single atom out-couplers. The latter aims to address the current challenge with stochastic loading of single atom traps. To date, the

best loading efficiency, which translates into the fill factor of an array, is 91% using collisional blockade [1]. This could be improved using a superconductor to Mott-insulator transition, but at the cost of experimental overhead and production rate [2]. A forward-looking possibility is to use single-atom out-couplers from a BEC. The portfolio of atom and potentially molecule candidates, albeit limited, is sizable and growing [3]. Future sources will be the focus of our theory explorations.

2 Theoretical Investigation of a Coherent Source

A model was developed for Bose-Einstein-condensate-based devices. To illustrate its application, a 2-well system is studied. The results show interesting and possibly useful differences between operation with coherent (phased-locked) and incoherent (unlocked) population transfer between levels in the two wells. The two modes of operation are governed by an interplay among scattering, energy renormalizations and coupling between wells.

2.1 Theory

The Hamiltonian may be divided into two parts:

$$H = H_0 + H_1 \tag{1}$$

The single-particle part is

$$H_0 = \frac{p^2}{2m} + V(r) \tag{2}$$

where $V(r)$ is the confinement potential describing the well combination, etc. (see solid curve Figure 2). The second term in (1)

$$H_1 = V(r_1, r_2) \tag{3}$$

describes particle-particle interaction which plays an important role in the population dynamics. For the modeling, we rewrite in terms of the uncoupled-well potentials $V_a(r)$ and $V_b(r)$:

$$\begin{aligned} H_0 &= \left[\frac{p_a^2}{2m} + V_a(\mathbf{r})\right] + \left[\frac{p_b^2}{2m} + V_b(\mathbf{r})\right] + [V(r) - V_a(r) - V_b(r)] \\ &= H_A + H_B + V_{AB} \end{aligned} \tag{4}$$

where we know the solutions to

$$\begin{aligned} H_A\phi_i^A(r) &= \varepsilon_i^A\phi_i^A(r) \\ H_B\phi_i^B(r) &= \varepsilon_i^B\phi_i^B(r) \end{aligned} \tag{5}$$

In our example, $V_a(\mathbf{r})$ and $V_b(\mathbf{r})$ are the dashed parabolas in Figure 2, giving simple-harmonic-oscillator solutions for ε_i^A, ε_i^B, $\phi_i^A(r)$ and $\phi_i^B(r)$ (blue curves).

Proceeding with the 2nd quantization, we have the state function,

$$\widehat{\psi}(r) = \sum_i a_i\phi_i^A(r) + \sum_j b_j\phi_j^B(r) \tag{6}$$

where $\phi_i^A(r)$ and $\phi_j^B(r)$ are localized at left and right wells, a_i and b_j are the annihilation operators for atoms in the j^{th} state in the left and right well, respectively. Using (6) and (4), we have, in second quantized form,

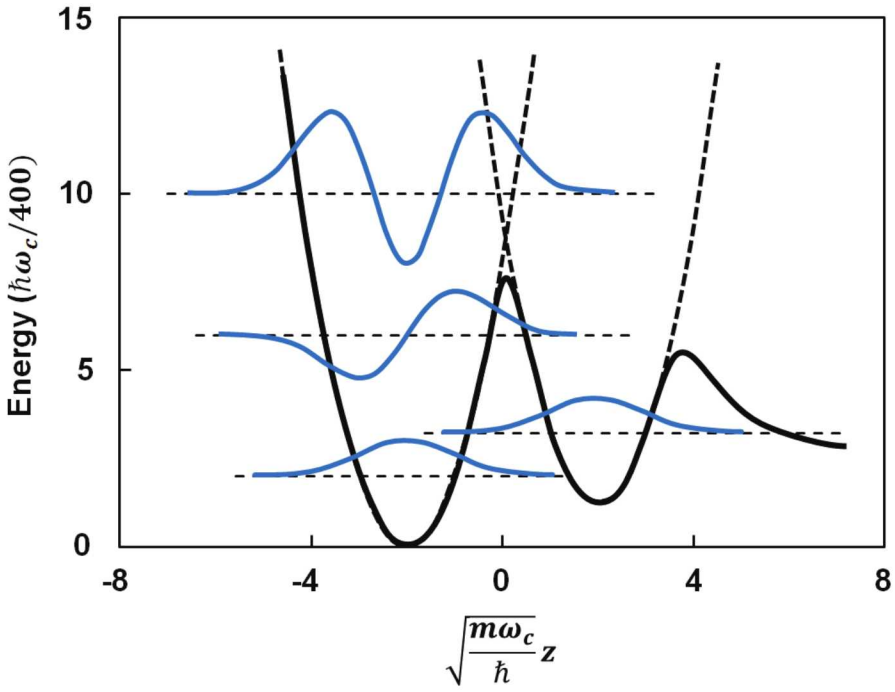

Figure 2: Confinement potential (black solid curve) for 2-well combination. The parabolas (black dashed curves) approximate the potentials for the uncoupled wells. The blue curves are the eigenfunctions for these simple harmonic potentials, displaced vertically according to their energies.

$$H_0 = \int \mathrm{d}^3\mathrm{r}\ \widehat{\psi}^\dagger(r)\left(H_A + H_B + V_{AB}\right)\widehat{\psi}(r)$$

and

$$H_1 = \int \mathrm{d}^3\mathrm{r}_2 \int \mathrm{d}^3\mathrm{r}_1\ \widehat{\psi}^\dagger(r_2)\widehat{\psi}^\dagger(r_1)V(r_1,r_2)\widehat{\psi}(r_1)\widehat{\psi}(r_2)$$

The end result is the following many-body Hamiltonian

$$\begin{aligned} H &= \sum_i \varepsilon_i^A a_i^\dagger a_i + \sum_j \varepsilon_j^B b_j^\dagger b_j \\ &\quad + \sum_{i,j}\left(g_{ij}a_i^\dagger b_j + h.a.\right) \\ &\quad + \sum_{i,j,k\neq 0}\left(v_{ijk}a_{i-k}^\dagger a_{j+k}^\dagger a_j a_i + h.a.\right) \end{aligned} \tag{7}$$

where

$$g_{ij} = \int \mathrm{d}^3\mathrm{r}\ \phi_i^A(r)V_{AB}\phi_j^B(r) \tag{8}$$

is a coupling coefficient due to the coupling of wells, and

$$v_{ijk} = \int \mathrm{d}^3\mathrm{r}_2 \int \mathrm{d}^3\mathrm{r}_1\ \phi_{i-k}^A(r_2)\phi_{j+k}^A(r_1)V(r_1,r_2)\phi_j^A(r_1)\phi_i^A(r_2) \tag{9}$$

accounts for atom-atom correlations leading to energy renormalizations and population relaxation. As will be seen later, the mean field contribution to last term in Eq. (7) accounts for the $\mathrm{U}_0\left|\psi\right|^2$ contribution in the Gross-Pitaevskii equation.

2.2 Equations of motion

Using (7) and the commutation relations

$$\left[a_i, a_j^\dagger\right] = \delta_{i,j} \tag{10}$$

$$\left[b_i, b_j^\dagger\right] = \delta_{i,j} \tag{11}$$

in

$$i\hbar\frac{\mathrm{d}O}{\mathrm{d}t} = [O,H] \tag{12}$$

we get with trunication at the Hartree-Fock level,

$$\frac{\mathrm{d}\left\langle a_i^\dagger a_i\right\rangle}{\mathrm{d}t} = \frac{i}{\hbar}\sum_j g_{ij}\left(\left\langle b_j^\dagger a_i\right\rangle - \left\langle a_i^\dagger b_j\right\rangle\right) \tag{13}$$

$$\frac{\mathrm{d}\left\langle b_j^\dagger b_j\right\rangle}{\mathrm{d}t} = -\frac{i}{\hbar}\sum_i g_{ij}\left(\left\langle b_j^\dagger a_i\right\rangle - \left\langle a_i^\dagger b_j\right\rangle\right) \tag{14}$$

$$\begin{aligned}\frac{\mathrm{d}\left\langle a_i^\dagger b_j\right\rangle}{\mathrm{d}t} &= \frac{i}{\hbar}\left(\Delta_{ji} + 4\sum_k v_{ijk}\left\langle a_{i-k}^\dagger a_{i-k}\right\rangle\right)\left\langle a_i^\dagger b_j\right\rangle \\ &\quad + \frac{i}{\hbar}g_{ij}\left(\left\langle b_j^\dagger b_j\right\rangle - \left\langle a_i^\dagger a_i\right\rangle\right)\end{aligned} \tag{15}$$

where $\Delta_{ji} = \varepsilon_j^B - \varepsilon_i^A$.

For the present model, we further simplify:

$$\left\langle a_i^\dagger a_i\right\rangle = n_i^A \tag{16}$$

$$\left\langle b_j^\dagger b_j\right\rangle = n_j^B \tag{17}$$

$$\left\langle a_i^\dagger b_j\right\rangle = \sqrt{n_i^A n_j^B}\exp\left[i\left(\theta_i^A - \theta_j^B\right)\right] \tag{18}$$

This gives

$$\frac{\mathrm{d}n_i^A}{\mathrm{d}t} = -\frac{2}{\hbar}\sum_j g_{ij}\sqrt{n_i^A n_j^B}\sin\theta_{ij} \tag{19}$$

$$\frac{\mathrm{d}n_j^B}{\mathrm{d}t} = \frac{2}{\hbar}\sum_j g_{ij}\sqrt{n_i^A n_j^B}\sin\theta_{ij} \tag{20}$$

$$\frac{\mathrm{d}\theta_{ij}}{\mathrm{d}t} = \frac{1}{\hbar}\left(\Delta_{ji} + 4\sum_k v_{ijk}n_{i-k}^A\right) + \frac{g_{ij}}{\hbar}\frac{n_j^B - n_i^A}{\sqrt{n_i^A n_j^B}}\cos\theta_{ij} \tag{21}$$

where $\theta_{ij} = \theta_i^A - \theta_j^B$ and $\Delta_{11} = \left(\varepsilon_1^A - \varepsilon_1^B\right)/\hbar$.

2.3 Correlation/collision effects

The next step is to include the pump and relaxation, with the latter arising from the higher correlations of H_1. Equations (19) to (21) then becomes

$$\frac{\mathrm{d}n_i^A}{\mathrm{d}t} = -\frac{2}{\hbar}\sum_j g_{ij}\sqrt{n_i^A n_j^B}\sin\theta_{ij} + \left.\frac{\mathrm{d}n_i^A}{\mathrm{d}t}\right|_{\text{col lisions}} + P_i \tag{22}$$

$$\frac{\mathrm{d}n_j^B}{\mathrm{d}t} = \frac{2}{\hbar}\sum_j g_{ij}\sqrt{n_i^A n_j^B}\sin\theta_{ij} + \left.\frac{\mathrm{d}n_i^B}{\mathrm{d}t}\right|_{\text{col lisions}} \tag{23}$$

$$\frac{\mathrm{d}\theta_{ij}}{\mathrm{d}t} = \frac{1}{\hbar}\left(\Delta_{ji} + 4\sum_k v_{ijk}n_{i-k}^A\right) + \frac{g_{ij}}{\hbar}\frac{n_j^B - n_i^A}{\sqrt{n_i^A n_j^B}}\cos\theta_{ij} \tag{24}$$

Following a treatment that has been successful in describing collisional effects in semiconductor devices, we have

$$\left.\frac{\mathrm{d}n_i^\sigma}{\mathrm{d}t}\right|_{\mathrm{col\,lisions}} = -\gamma\left[n_i^\sigma - f\left(\varepsilon_i^\sigma, \mu, T\right)\right] \tag{25}$$

where γ is an effective collision rate. In this treatment, n_i^σ is the actual population of the ith level in the σ well, according to loading, evaporation and collision effects, $f\left(\varepsilon_i^\sigma, \mu, T\right)$ is the equilibrium population that it relaxes to in the limit of infinite γ. In our case, $f\left(\varepsilon_i^\sigma, \mu, T\right)$ is given by a Bose-Einstein function with chemical potential μ and temperature T, determined by the conservation of total atomic population and energy:

$$\sum_i n_i^\sigma = \sum_i f\left(\varepsilon_i^\sigma, \mu, T\right) \tag{26}$$

$$\sum_i \varepsilon_i^\sigma n_i^\sigma = \sum_i \varepsilon_i^\sigma f\left(\varepsilon_i^\sigma, \mu, T\right) \tag{27}$$

2.4 Results from modeling

In the simulations, we consider a situation where the ground state of the left well is initially occupied, together with a very small background population in the other states. Atoms are injected into the 5th level and removed at the 6th level of the left well. The time evolution of the populations is investigated in the presence of loading, evaporation, drain, scattering and well-to-well coupling.

Unique to a BEC system is the presence of relative phases between levels. Central to the results is the behavior of the relative phase between the ground states of the left and right wells:

$$\phi \equiv \theta_1^A - \theta_1^B \tag{28}$$

Figure 3 shows the beatnote $\mathrm{d}\phi/\mathrm{d}t$ for two values of locking parameter $g_{11} = 0.07$ and 0.08. Also plotted is the detuning, $\left(\Delta_{11} + 4v_{110}\left(n_1^A - n_1^B\right)\right)(\hbar\gamma)^{-1}$. For the smaller locking parameter, the phases are unlock, while for the larger locking parameter, locked operation occurs after $\gamma t \simeq 4000$. The locking arises from the increase in population n_1^A, which causes the detuning to decrease because of the exchange shift proportional to v_{110}.

The significance between locked and unlocked operation clearly shows up in the rate of atoms outcoupled from the system. In Fig. 4, this rate, $\gamma_{out} n_1^B$ is plotted as a function of time for the two locking parameters. For the higher locking parameter, one sees a drastic increase in $\gamma_{out} n_1^B$ after the onset of locking.

Figure 5 contains plots of the spatial distributions of the atomic population given by,

$$\left\langle \widehat{\psi}^\dagger(r)\widehat{\psi}(r)\right\rangle = \left|\phi_1^A(r)\right|^2 n_1^A + \left|\phi_1^B(r)\right|^2 n_1^B + 2\sqrt{n_i^A n_j^B}\,\mathrm{Re}\left\{\left[\phi_i^A(r)\right]^* \phi_j^B(r)\exp\left[i\phi\right]\right\} \tag{29}$$

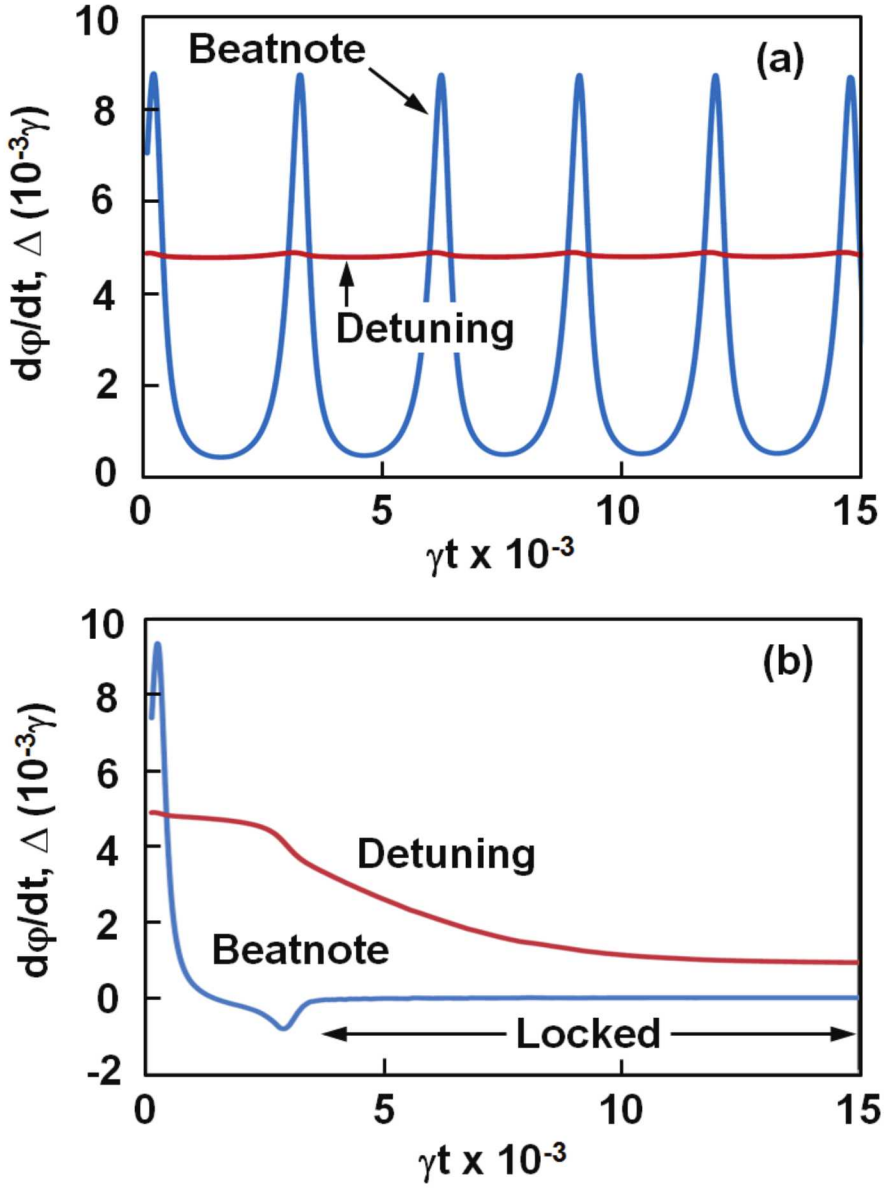

Figure 3: Time evolution of beatnote (blue curve) and detuning (red curve) between ground state populations of the two wells for (a) unlocked and (b) locked operation.

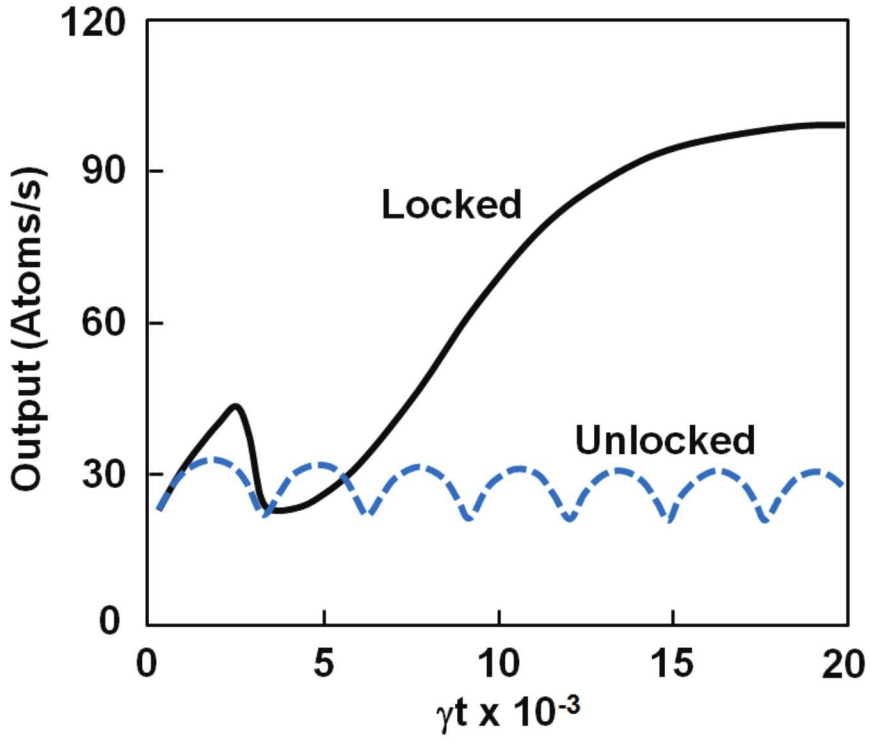

Figure 4: Difference in output between unlocked (dashed curve) and locked (solid curve) operation.

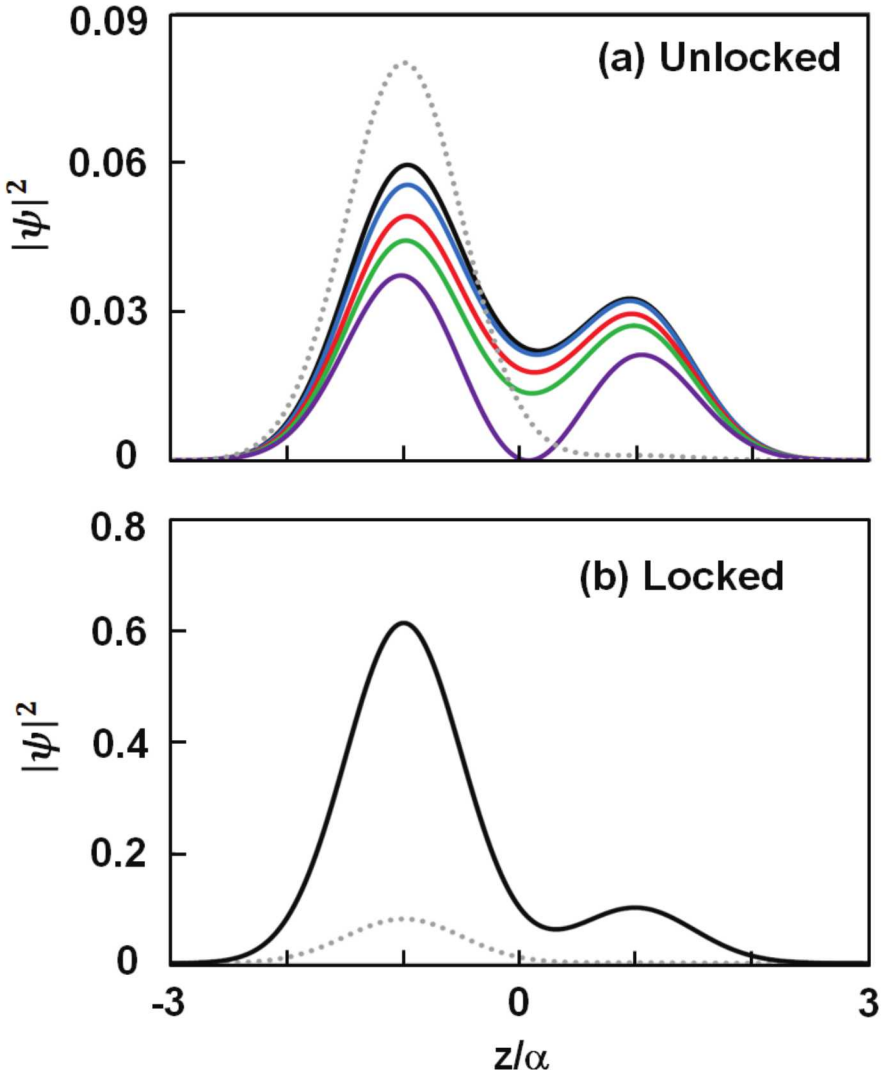

Figure 5: Spatial distribution of atoms under (a) unlocked and (b) locked operation after steady state is reached. The starting distributions are identical in both cases (dotted grey curves). Note the significant difference in the ordinate scaling. For unlocked operation, the distribution oscillates among the solid curves. For locked operation a time independent distribution is reached.

The dotted curve is the initial distribution, identical for both locked and unlocked cases, and localized in left well. The solid curves show the distributions after steady state is reached. In the case of unlocked operation (Fig. 5(a)), the population oscillates between the nondegenerate eigenstates $\phi_1^A(r)$ and $\phi_1^B(r)$, producing the different shapes shown by the solid curves. In the locked case, a composite eigenstate is formed, giving a time-independent spatial distribution, shown in Fig. 5(b).

Some clue into the cause of the improvement in atom transfer from left to right well may come from the time evolution of the population in each level. The blue curve in Fig 6(a) shows the population distribution at an early time. The system is far from equilibrium, with a peak at the sixth level because of pumping. With time, relaxation takes place and after $\gamma t = 500$, the populations settle to essentially a Bose-Einstein distribution, with some deviations at the pump and extraction levels, and some fluctuations whose boundaries are indicated by the red and green curves.

In the beginning, a similar progression is followed by the locked case. First, the rise in temperature (decrease in slope), with population of the higher lying states, including that of the right well, as depicted by the grean and red data. Then with the onset of locking, significant cooling takes place, even while the total atom population continues to grow appreciably (compare red to blue and black data). Time independence occurs at around $\gamma t = 1000$.

Figure 7 summarizes the results presented in Fig. 6. In Fig. 7(a), we plotted the time evolution of the fraction of ground state population versus the sum of populations in the other states for the well. In Fig. 7(b), we plotted the effective temperature, which is obtained from fitting the population distribution to an equivalent Bose-Einstein function. The curves show significant BEC in the locked system, compared to that of the unlocked one.

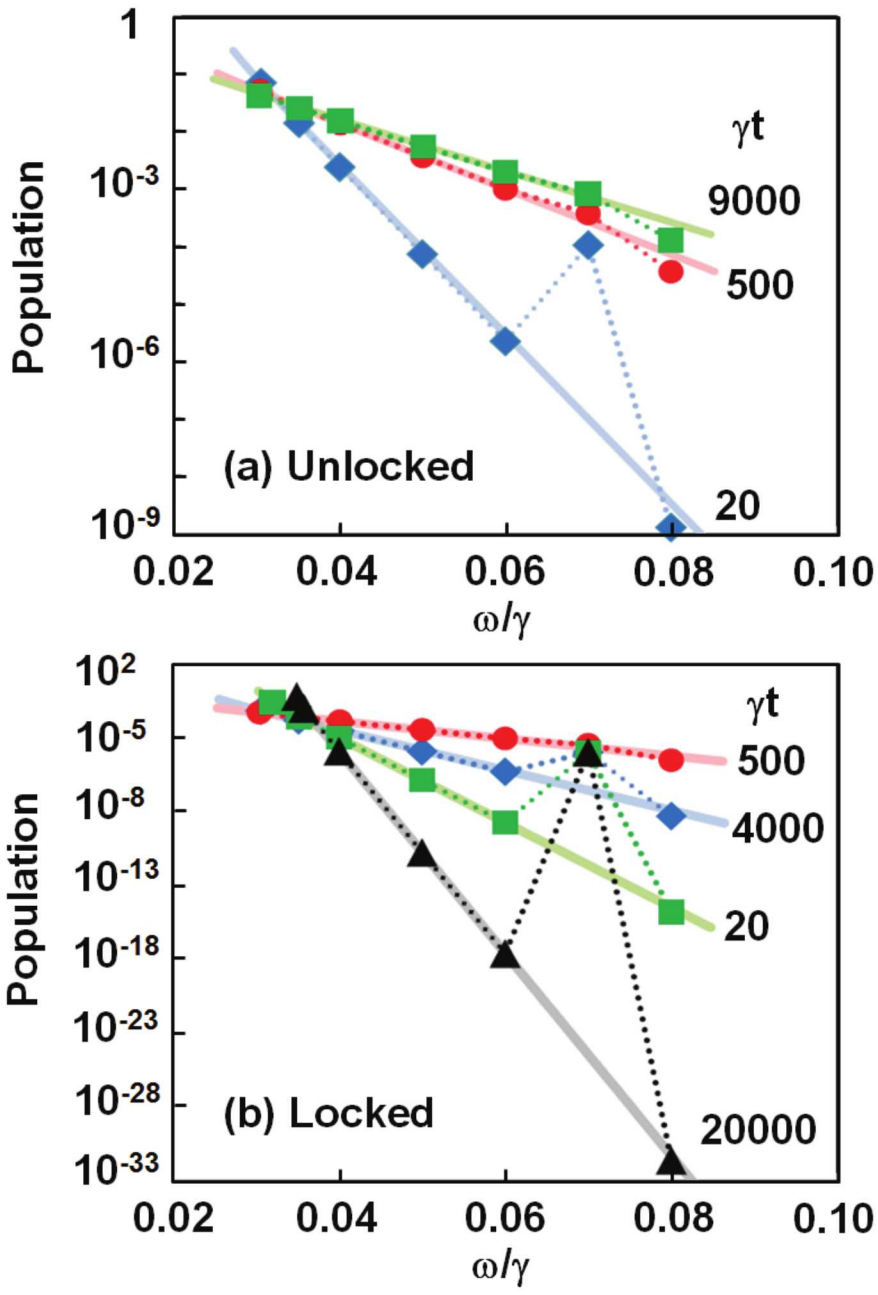

Figure 6: Time evolution of atomic distributions for (a) unlocked and (b) locked operation. Atoms are injected in the second highest level and removed from the highest level. The solid straight lines show the Bose-Einstein distributions with equivalent total populations and energies.

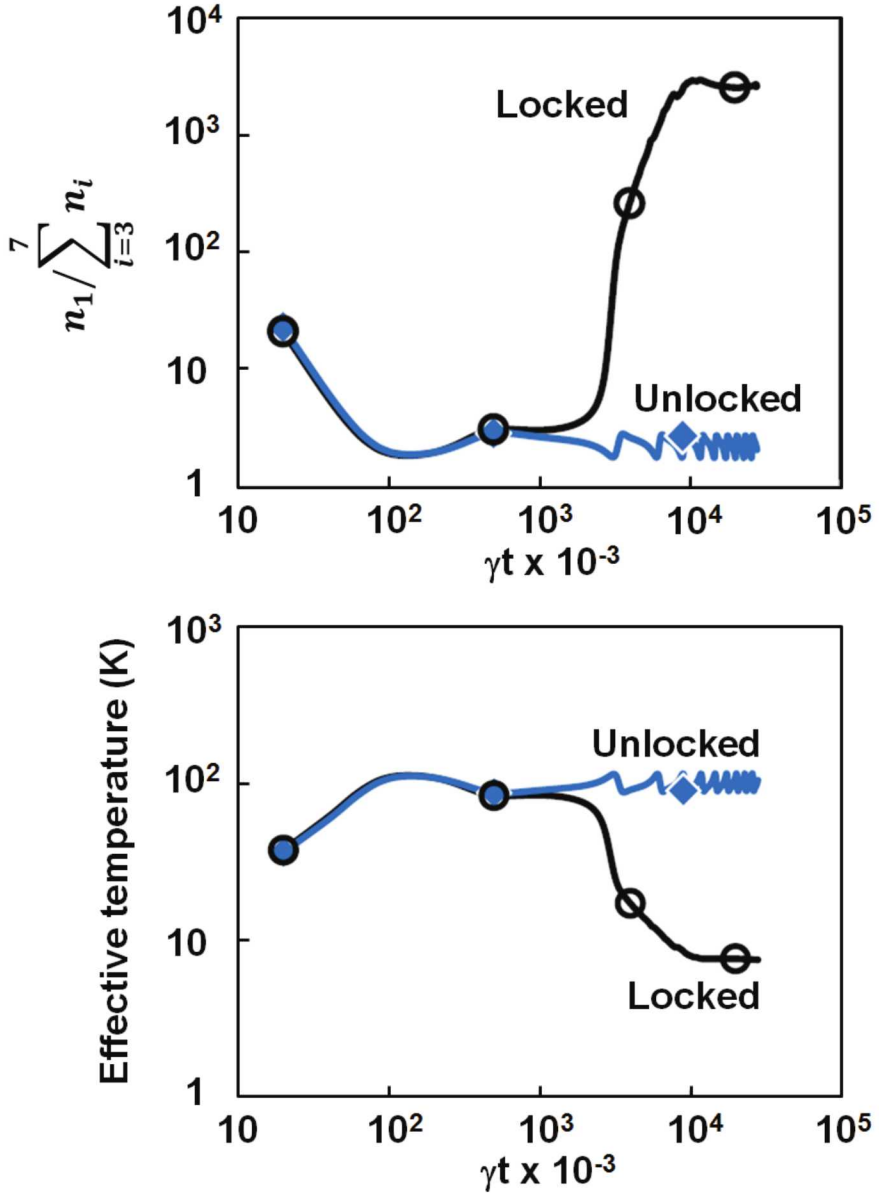

Figure 7: Time evolution of (a) condensation and (b) effective temperature of populations in the left well for unlocked (blue curve) and locked (black curve) operation. The filled diamonds and unfilled circles indicate the times for the distributions plotted in Fig. 6.

3. EXPERIMENTAL INVESTIGATION OF ATOM DEPOSITION TECHNIQUES

One approach for deposition on a surface is to translate the atom from a trap loading location in vacuum chamber to the surface. Approaching the surface is supported by recent work that positioned a rubidium atom 260 nm from a photonic crystal surface using optical tweezers [4]. In our application, the Casimir-Polder force at this distance, exceeding 1000 m/s^2, could aid the remaining trap to surface transit. Migration of the deposited atom can be controlled by cooling the substrate to liquid helium temperatures [5]. In future work, single atom detection could be guaranteed with an ultra-high vacuum and low-temperature scanning probe microscope, and adapting this apparatus to accommodate single-cesium atom trapping and placement [6]. In this work, we determined the maximum translation rate for stepwise translation of a single cesium atom in a micron-scale optical tweezers.

The apparatus used to measure this rate is described in [7]. We adapt this apparatus for our purposes by adding a translation function to the control routine. The optical tweezers is created by a 938 nm laser that passes first through an AOM and then an aspheric lens with a focal length of 2.75 mm. By changing the drive frequency to the AOM, we change the deflection angle of the light and thus the position in the lens focal plane of the spot forming the optical tweezers. We measured the probability of atom retention following translation over 1.83 μm as a function of step size. It was found that for steps larger than 0.09 μm the atom loss increases significantly. A maximum translation rate of 45 mm/s was demonstrated which is sufficient for moving single atoms macroscopic distances in vacuum-limited lifetimes (typically 10 s or more).

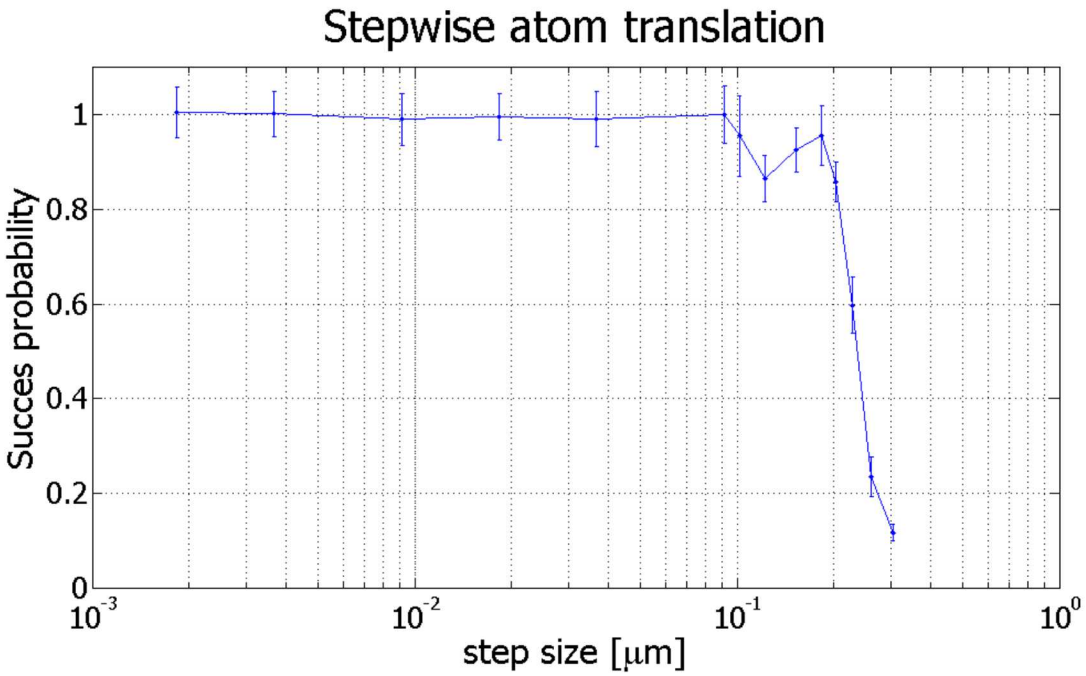

Figure 8: Success probability following atom translation as a function of step size. Steps are spaced by 2 μs. The fastest rate achieved was 45 mm/s. The source of the null near 0.11 μm may be caused by resonant excitation of a trap mode.

Recognizing that translation of the atom is limited by translation rate as discussed above, and that surface reflections cause standing waves that trap the atom above the surface [4], we seek an alternative method for our future demonstration of deposition, employing instead substrate translation of a transparent material as a first experiment.

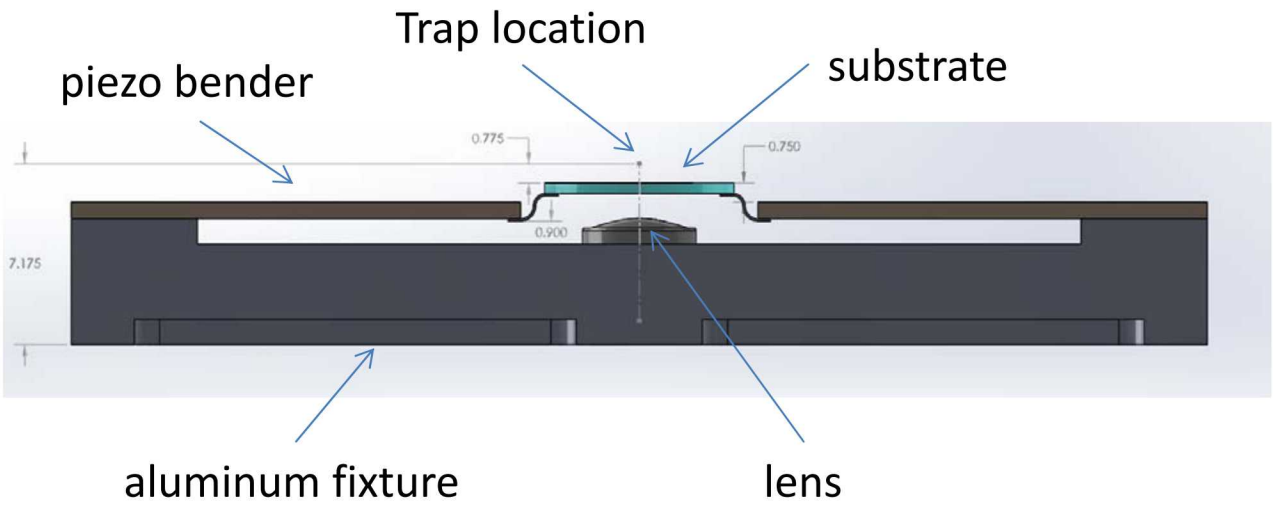

Figure 9: Solid model of the substrate translation scheme. The atom can be trapped above the substrate in an optical tweezers loaded from a mirror MOT [8]. Dimensions are in mm.

As depicted in Figure 9, the atom can be trapped in an optical tweezers above a surface using a magneto-optical trap with cooling light reflected from the surface. The substrate is transparent to the optical tweezers wavelength allowing the trap-forming lens to be located on the backside of the substrate and the tweezers are formed by focusing the light through the substrate to form a focus on the far side. The piezo benders are bi-directional with a displacement of order +/- 1 mm. During this stage, the surface is translated down close to the aspheric lens to provide room for the laser cooling dynamics. After the optical tweezers is loaded, the surface is translated toward the atom until the atom collides with the surface.

We have constructed the apparatus for this experiment as shown in Figure 10. The substrate in our apparatus is sapphire that is coated with platinum except for a narrow strip through which the tweezers light penetrates. The platinum provides a reflective surface for the mirror MOT. Future work should determine the efficacy of this approach for translating the substrate without perturbing the single atom. Ultimately, future investigations must determine a method for preparing a single trapped atom in the vicinity of a surface without decorating the surface with cesium adsorbates.

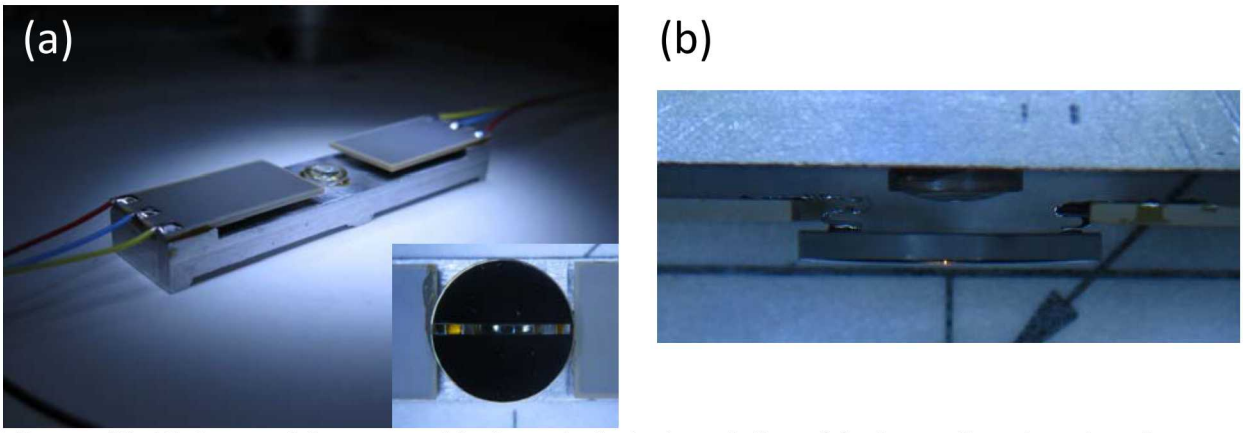

Figure 10: Pictures of the assembly for substrate translation. (a) shows the piezo benders and aluminum fixture without substrate attached. Inset: top view of the attached sapphire substrate with platinum coating. (b) Side view of the attachment of the substrate to the piezo benders provided by a flexible spring as it is suspended above the trapping lens.

4. CONCLUSION

We have theoretically and experimentally investigated the possibility of single atom deposition using laser cooled sources. In our theoretical work, we investigated an atom source composed of out-coupling from a Bose-Einstein condensate in a trap. A model was developed for Bose-Einstein-condensate-based devices. To illustrate its application, a 2-well system is studied. The results show interesting and possibly useful differences between operation with coherent (phased-locked) and incoherent (unlocked) population transfer between levels in the two wells. The two modes of operation are governed by an interplay among scattering, energy renormalizations and coupling between wells. In parallel, we have experimentally investigated the possibility of controlled deposition of single cesium atoms onto surfaces using optical tweezers. We have measured the rate limit for translation of single atoms in optical tweezers and have constructed an apparatus for deposition of single atoms on a sapphire substrate for future work. Future work could employ our approach to determine the Casimir-Polder interaction of a single atom probe with a surface by studying the variation of atom loss with surface proximity or using force-sensitivity atom interferometry with single atoms [9].

BIBLIOGRAPHY

1. Carpentier, et al., High efficiency preparation of single trapped atoms using blue detuned light assisted collisions. arXiv:1208.0707
2. Bakr, et al., A quantum gas microscope for detecting single atoms in a Hubbard-regime optical lattice. Nature 462, 74-77 (5 November 2009)
3. Rohwedder, Resource Letter AON-1: Atom optics, a tool for nanofabrication. Am. J. Phys. 75, 394 (2007) | doi: 10.1119/1.2673209
4. J. D. Thompson, et al., Coupling a Single Trapped Atom to a Nanoscale Optical Cavity, Science, 340, 1202 (2013)
5. Song, et al., Charge-transfer-induced cesium superlattices on graphene. Phys. Rev. Lett. 108, 156803 (2012)
6. Tantussi, et al., Towards laser-manipulated deposition for atom-scale technologies. Applied Surface Science 255, 9665–9670, (2009)
7. A. M. Hankin, et al., "Two-atom Rydberg blockade using direct 6S to nP excitation", Phys. Rev. A 89, 033416 (2014)
8. J. Reichel, et al., Atomic micromanipulation with magnetic surface traps, PRL, 83, 3398 (1999)
9. Parazzoli, et al., Observation of Free-Space Single-Atom Matterwave Interference. Phys. Rev. Lett. 109, 230401 (2012)

Distribution

1	MS0899	Technical Library	9536 (electronic copy)

For LDRD reports, add:

1	MS0359	D. Chavez, LDRD Office	1911

Sandia National Laboratories